SI Appendix

I. Magnetic Scattering Theory

As measurements were made on the Ni L_3 absorption edge on the purely magnetic (¼ ¼ ¼) peak, we will only consider the contribution of electric dipole transitions to the magnetic cross section. From Hill and McMorrow (1), the atomic scattering amplitude is then given by

$$f_n = \left[(\hat{\boldsymbol{\varepsilon}}' \cdot \hat{\boldsymbol{\varepsilon}})F^{(0)} - i(\hat{\boldsymbol{\varepsilon}}' \times \hat{\boldsymbol{\varepsilon}}) \cdot \widehat{\boldsymbol{m_n}}F^{(1)} + (\hat{\boldsymbol{\varepsilon}}' \cdot \widehat{\boldsymbol{m_n}})(\hat{\boldsymbol{\varepsilon}} \cdot \widehat{\boldsymbol{m_n}})F^{(2)}\right] \quad \text{(S1)}$$

where $\hat{\boldsymbol{\varepsilon}}$ and $\widehat{\boldsymbol{\varepsilon}'}$ are the polarizations of the incident and scattered light, $\widehat{\boldsymbol{m_n}}$ is the orientation vector of the magnetic moment of the n[th] ion, and $F^{(j)}$ are respective strengths of the three scattering processes. Again, as we are studying a magnetic reflection, the contribution of the first process will be zero. In a specular reflection geometry, this expression becomes Equation 15 of SI Appendix Reference 1. The atomic scattering factors for incident *p*-polarized light and scattered *s*- and *p*-polarized light are then respectively

$$f_{n,\pi\sigma} = \left[-iF^{(1)}\left(m_{n,3}\sin\theta - m_{n,3}cos\theta\right) + F^{(2)}\left(m_{n,2}\left(m_{n,1}\sin\theta + m_{n,3}cos\theta\right)\right)\right] \quad \text{(S2)}$$

$$f_{n,\pi\pi} = \left[-iF^{(1)}m_{n,2}\sin 2\theta - F^{(2)}\cos^2\theta\left(m_{n,1}^2\tan^2\theta + m_{n,3}^2\right)\right], \quad \text{(S3)}$$

and $\widehat{\boldsymbol{m_n}} = m_{n,1}\hat{\boldsymbol{\imath}} + m_{n,2}\hat{\boldsymbol{\jmath}} + m_{n,3}\hat{\boldsymbol{k}}$.

The Ni magnetic moments in the static AFM ordering of $NdNiO_3$ follows a ↑→↓← pattern along the [111] direction, where ↑ and ↓ are parallel to [111], while → and ← are along [-1-12]. In our scattering geometry, $\hat{\boldsymbol{k}}$ is parallel to [111], and we will define $\hat{\boldsymbol{\imath}}$ to be along [-1-12]. Then the magnetic moments for the four ions in the static magnetic unit cell are $\widehat{\boldsymbol{m}}_{\uparrow,\downarrow} = \pm m\hat{\boldsymbol{k}}$ and $\widehat{\boldsymbol{m}}_{\rightarrow,\leftarrow} = \pm m\cos\psi\,\hat{\boldsymbol{\imath}} \pm m\sin\psi\,\hat{\boldsymbol{\jmath}}$, where ψ is the angle between the incident wave vector projection into the plane and [-1-12].

The total scattering factor from a crystal for the π-to-σ scattering polarization is found from summing over all of the atomic layers according to

$$A_{\pi\sigma}(q) = \sum_n f_{n,\pi\sigma}\exp(-i2\pi q z_n), \quad \text{(S4)}$$

where q is the magnitude of the scattering vector and z_n is the position of the n[th] layer. The ionic position can be decomposed into the sum of the position a scattering cell, z_p, and the place of this layer within the cell, z_r, where $z_n = z_p + z_r$. The crystal scattering factor then takes the form

$$A_{\pi\sigma}(q) = \sum_p \sum_r f_{p,r,\pi\sigma}\exp(-i2\pi q z_r)\exp\left(-i2\pi q z_p\right) = \sum_p F_{p,\pi\sigma}\exp\left(-i2\pi q z_p\right). \quad \text{(S5)}$$

If the magnetic scattering cell is also allowed to deform by different amounts as a function of depth, the position of the p-th cell can be written as $z_p = pz_u + \Delta_p$, where z_u is the ideal cell spacing and Δ_p is the displacement or strain of the p-th cell. This expression can be inserted into Eqn. (S5), resulting in

$$A_{\pi\sigma}(q) = \sum_p F_{p,\pi\sigma}\exp\left(-i2\pi q\Delta_p\right)\exp(-i2\pi q p z_u) \quad \text{(S6)}$$

This sum can be expressed as an integral over z, then the crystal scattering factor becomes

$$A_{\pi\sigma}(q) = \int F_{\pi\sigma}(z)\exp(-i2\pi q\Delta(z))\exp(-i2\pi q z)dz \quad \text{(S7)}$$

The same expression can be written for the $\pi\pi$ polarization amplitude, following the same arguments. The observed intensity is then the incoherent sum of the intensity from the two scattering polarizations,

$$I(q) = |A_{\pi\sigma}(q)|^2 + |A_{\pi\pi}(q)|^2. \quad \text{(S8)}$$

Summing over a single unit cell, using Equations (S2), (S3) and the magnetic moments defined previously, the expressions for the scattering factors of the ¼ ¼ ¼ reflection are

$$F_{\pi\sigma} = 2mf_{Ni}(\sin\theta + i\cos\theta\cos\psi), \quad \text{(S9)}$$
$$F_{\pi\pi} = 2mf_{Ni}i\sin 2\theta\sin\psi. \quad \text{(S10)}$$

In these expressions, we define the variable f_{Ni} as equivalent to $F^{(1)}$ for nickel in the notation that was used in Equations (S2) and (S3) from SI Reference 1. The terms proportional to $F^{(2)}$ were found to cancel out for this reflection.

As the resolution in this experiment is larger than a unit cell, we will consider a larger scattering cell consisting of some number of unit cells, *N*. We will let the magnetization in each cell vary, leading to a z-dependence on the scattering factor as in Equation (S6). Now we will also describe the changes in magnetization in each scattering cell in terms of the projection of the average moment at each depth onto the static magnetization orientation. That is to say, we assume that the orientation angles of the moment (θ and ψ) are not z dependent. The scattering factor profiles then become

$$F_{\pi\sigma}(z) = 2Nf_{Ni}m(z)(\sin\theta + i\cos\theta\cos\psi), \quad \text{(S11)}$$
$$F_{\pi\pi}(z) = 2Nf_{Ni}m(z)i\sin 2\theta\sin\psi \quad \text{(S12)}$$

From Equation (S8), it is then found that the observed intensity becomes

$$I(q) = 4N^2{f_{Ni}}^2\alpha^2(\theta,\psi)\left|\int m(z)\exp(-i2\pi qz)dz\right|^2 \quad \text{(S13)}$$

and the scattering amplitude is

$$A(q) = 2Nf_{Ni}\alpha(\theta,\psi)\int m(z)\exp(-i2\pi qz)dz \quad \text{(S14)}$$

where

$$\alpha(\theta,\psi) = (sin^2\theta + cos^2\theta\, cos^2\psi + sin^2 2\theta\, sin^2\psi)^{1/2} \quad \text{(S15)}$$

If we ignore the incoherent sum in the iterative phase retrieval, we are treating the observed intensity originating from a single scattering factor profile as

$$I(q) = \left|\int_{-\infty}^{\infty} f(z)\, e^{2\pi iqz}\, dz\right|^2 \quad \text{(S16)}$$

and the amplitude is then

$$A(q) = \int_{-\infty}^{\infty} f(z)\, e^{2\pi iqz}\, dz. \quad \text{(S17)}$$

Then from equation S13, the obtained scattering factor profile is related to the magnetization profile by

$$f(z) = 2\, Nf_{Ni}\alpha(\theta,\psi)m(z). \quad \text{(S18)}$$

In general, $f(z)$ is assumed to be a complex function, leading to the expression

$$f(z) = 2\, Nf_{Ni}\alpha(\theta,\psi)m(z)e^{i\phi(z)}. \quad \text{(S19)}$$

So, $m(z)$ is proportional to the amplitude of the obtained scattering factor profile function recovered by iterative phasing algorithms. The phase profile $\phi(z)$ can be related to the strain profile, $\Delta(z)$, as shown in Equation (S7), however, next I will also show that under different assumptions it can also be related to the magnetization orientation profile.

Now assuming that the magnetization orientation angles are also dependent on the position in the film leads to a scattered intensity of the form

$$I(q) = 4N^2{f_{Ni}}^2\left[\left|\int m(z)\left(\sin^2\theta(z) + \cos^2\theta(z)\cos^2\psi(z)\right)\exp\left(-i2\pi qz + i\phi_{\pi\sigma}(z)\right)dz\right|^2 + \left|\int m(z)(\sin^2 2\theta(z)\sin^2\psi(z))\exp(-i2\pi qz + \pi/2)dz\right|^2\right] \quad \text{(S20)}$$

where $\phi_{\pi\sigma}(z) = \arctan(\cot\theta\,(z)\cos\psi(z))$.

While this is a more general treatment, the real space amplitude from each polarization is found to be a complicated product of three z-dependent functions. The separation of the

recovered amplitude into these respective functions is not possible without multiple measurements at different incident beam ψ angles for each time delay. Furthermore, applying phase retrieval to an incoherent sum of the amplitudes from the two polarizations will recover some complex average of them (2). Therefore, we will not consider this model as it does not allow for a clear physical interpretation of the results. As a corollary, we cannot differentiate from our analysis if the $m(z)$ profile recovered assuming Equation (S19) is truly due to a position dependence of the magnetic moment magnitude, or its orientation. Also, it becomes unclear if the recovered phase profile is due to a strain profile, or somehow related to $\phi_{\pi\sigma}(z)$ from Equation (S14).

II. Iterative Phase Retrieval Projection Operators

An error-reduction algorithm was used to recover the amplitude and phase of the real space scattering profiles. One iteration of the algorithm updated the recovered the real space scattering profile, $f(z)$, by applying a reciprocal space modulus projection, $\boldsymbol{P_m}$, followed by a real space support projection, $\boldsymbol{P_s}$, as in

$$f_{n+1}(z) = \boldsymbol{P_s P_m} f_n(z)\ . \tag{S21}$$

The support projection is defined as

$$\boldsymbol{P_s} f_n(z) = \begin{cases} f_n(z) & \text{if } z \in S \\ 0 & \text{otherwise} \end{cases}, \tag{S22}$$

where S is the set of points belonging to the support

The modulus projection was defined as

$$\boldsymbol{P_m} = \mathcal{F}^{-1}\widetilde{\boldsymbol{P}}_{\boldsymbol{m}}\mathcal{F} f_n(z) \tag{S23}$$

with $\mathcal{F}$ denoting the fourier transform operation and $\widetilde{\boldsymbol{P}}_{\boldsymbol{m}}$defined as

$$\widetilde{\boldsymbol{P}}_{\boldsymbol{m}} = A(q)e^{i\phi_n(q)} \tag{S24}$$

where $A(q)$ is the modulus of the measured intensity and $\phi_n(q)$ is the phase of $\mathcal{F} f_n(z)$. As described in the manuscript, this sequence of projections was repeatedly applied until convergence of $f(z)$ was reached.

III. L-curve support determination

A fixed support size was determined for each time delay by conducting a trial of phase retrieval for different support sizes, L, and recording the converged values of the residual metric, R, defined in Equation (6). The support size was chosen as that corresponding to the bend in the $R(L)$ curve. Examples of such curves for a few time delays are depicted in Figure S1. For the -0.5 ps time delay data, the support size of 30 nm was used, while for 5.5 ps a support size of 17 nm was used.

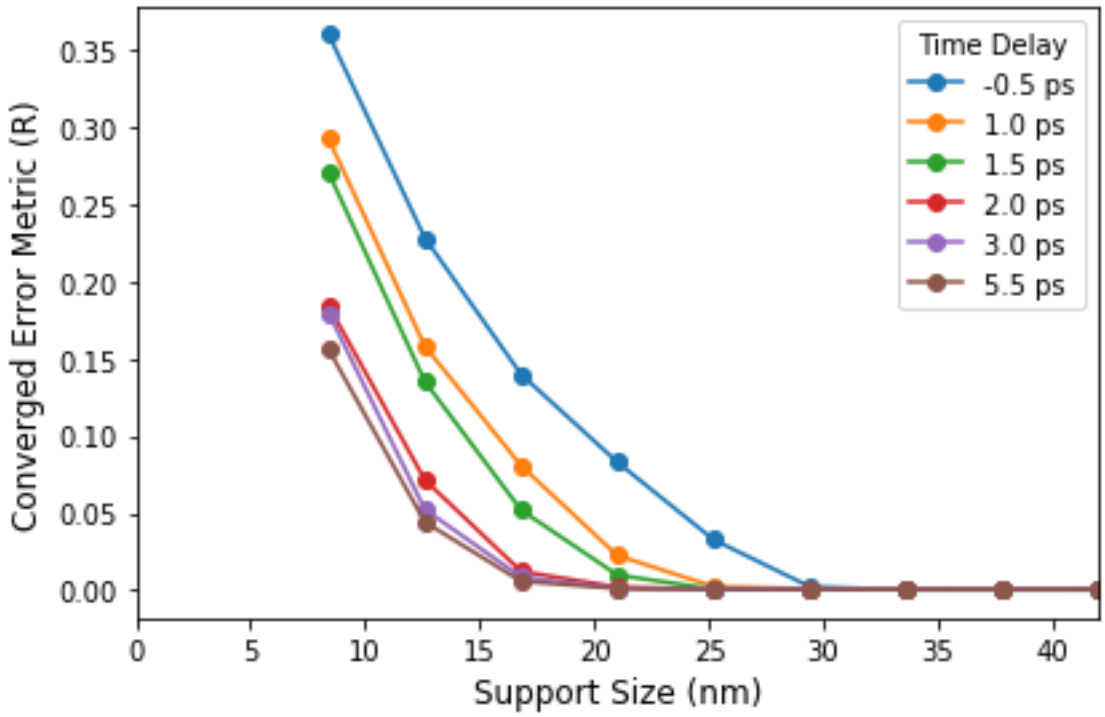

Figure S1. Trends of the converged values of the error metric assuming different support sizes.

IV. Magnetization Recovery Dynamics

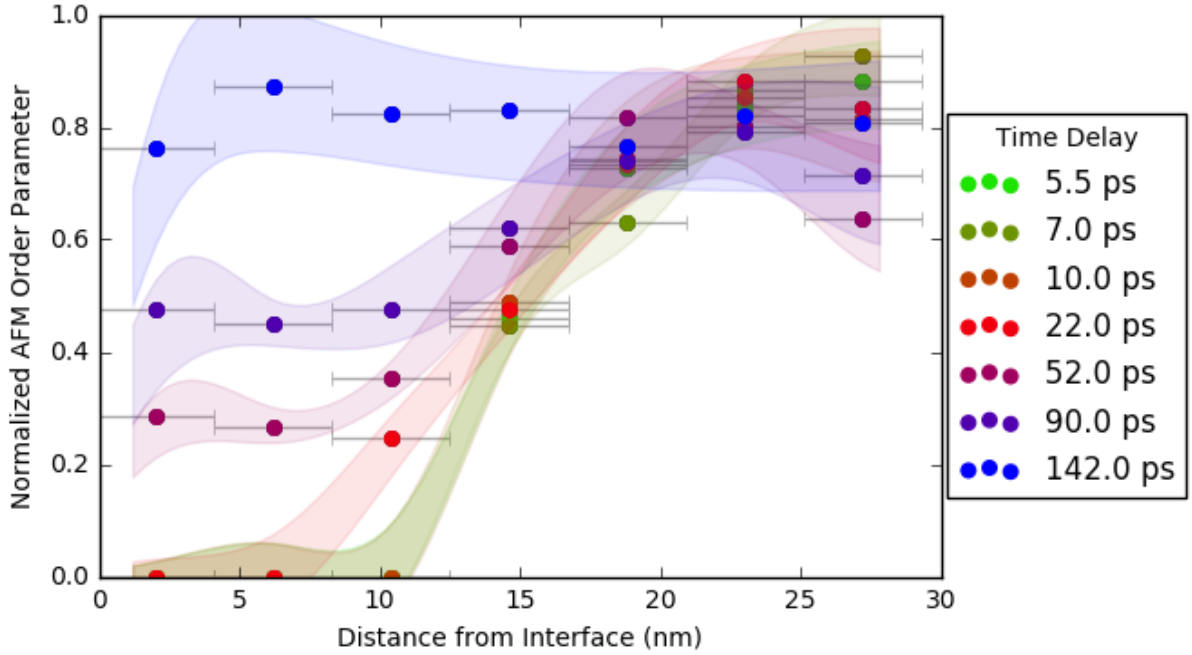

Figure S2. Magnetization profiles for long time delays after mid-IR excitation. Starting from the last time delay in Figure 3a, images of the AFM ordering recovery in the film after mid-IR excitation of the substrate are shown. The magnetization only begins to recover after 22 ps, and is nearly fully recovered after 142 ps.

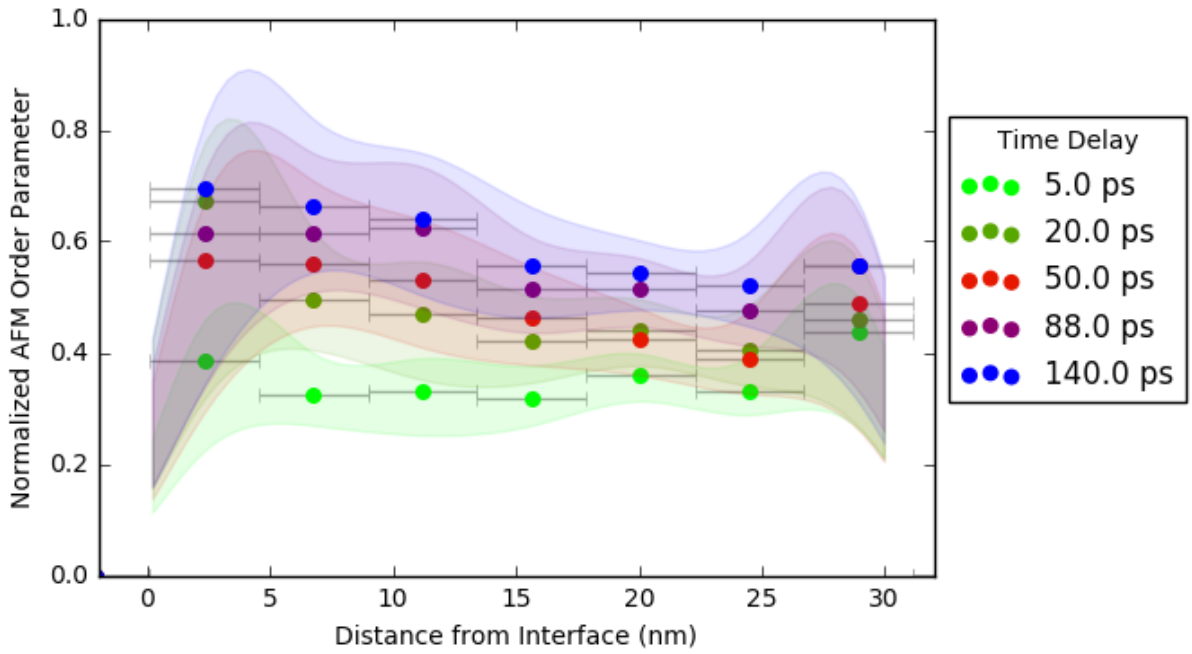

Figure S3. Magnetization profiles for long time delays after 800nm excitation. Starting from the last time delay in Figure 3b, images of the AFM ordering recovery in the film after 800nm excitation of the film are shown. Even after 142 ps, the magnetization has only recovered to about 60% of its equilibrium value.

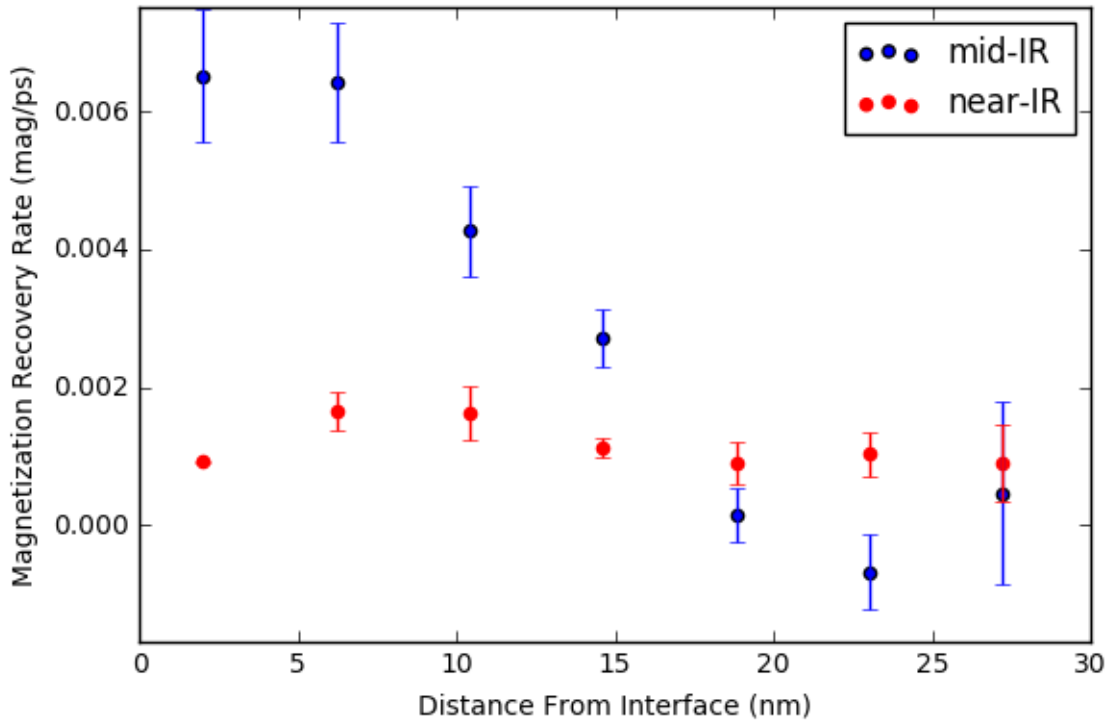

Figure S4. Rate of magnetization recovery as a function of position in the film for mid-infrared and near-infrared excitations. The normalized magnetization profiles from Figure S1 and S2 for time delays longer than 20 ps were analyzed to obtain the rate of recovery as a function of distance from the interface. Trends for this magnetization as a function of time at each position in the film were fit to a linear model, the slope of which is defined as the magnetization recovery rate.

V. Recovered Phase Profiles

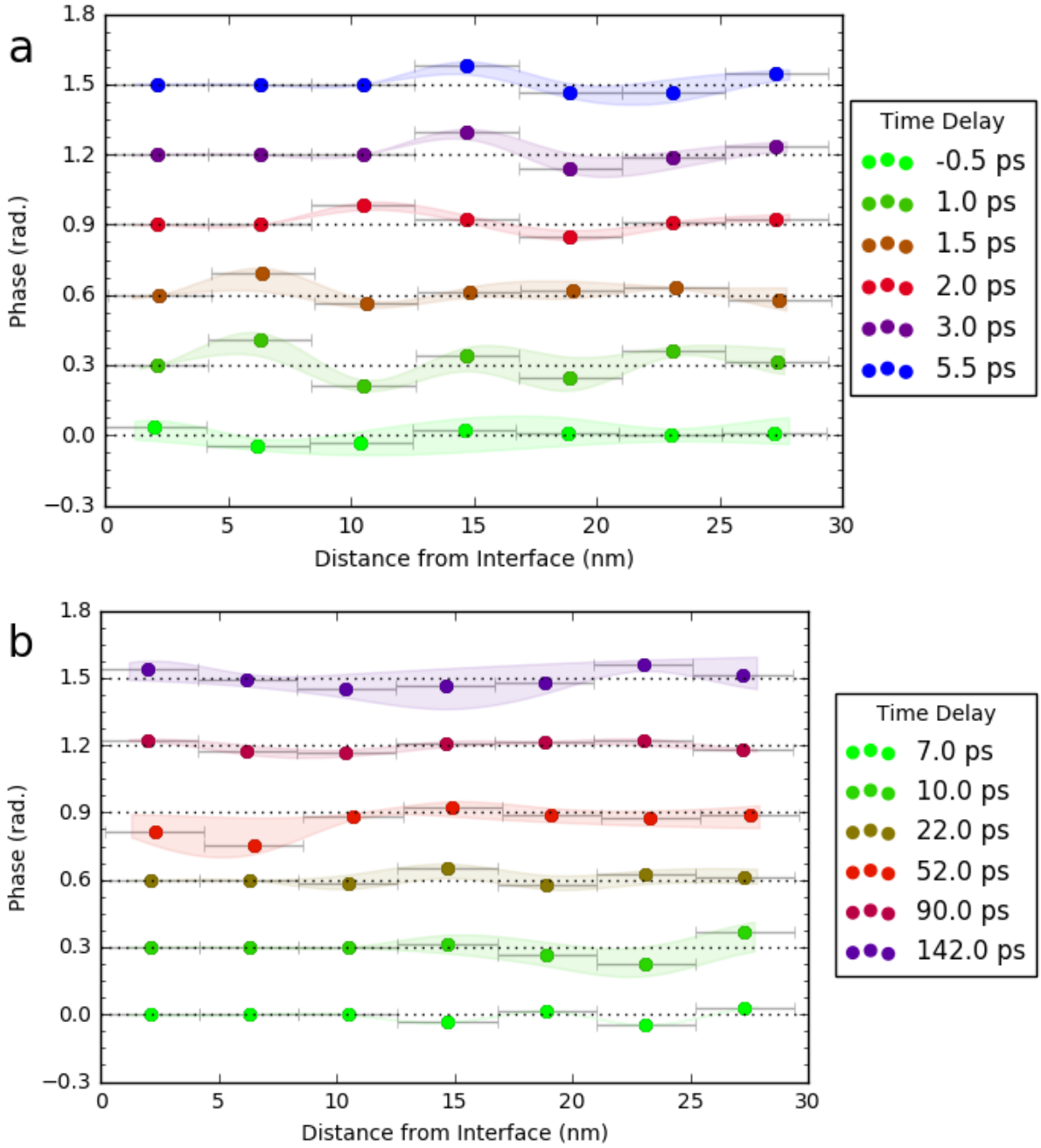

Figure S5. Recovered phase profiles for different time delays after mid-infrared excitation. Each profile has been offset for clear presentation and the dotted lines denote each respective zero phase line. (a) The phase profiles from Figure 3a, and (b) Figure S2 are during the early and later times of the magnetization recovery process are shown.

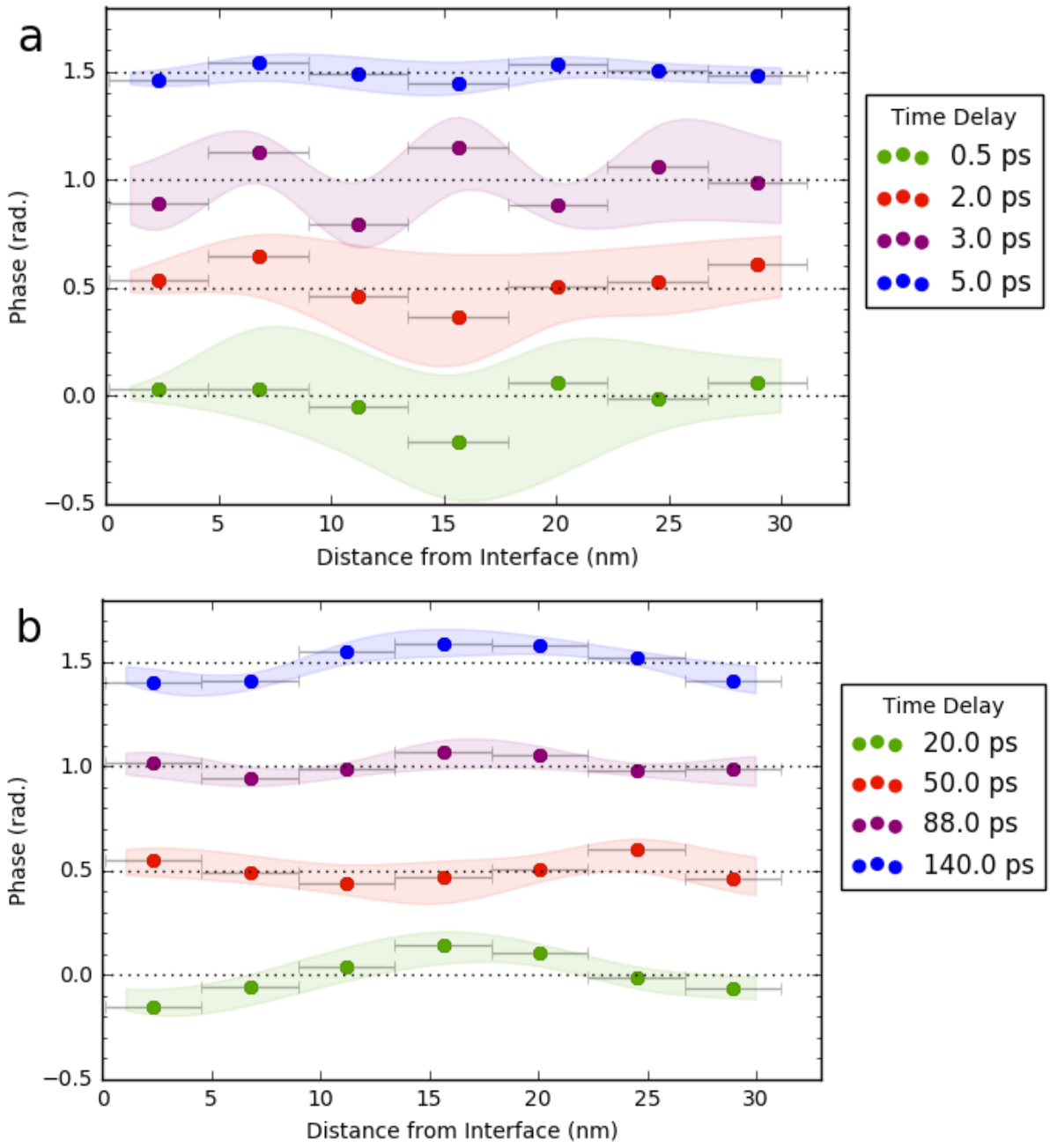

Figure S6. Recovered phase profiles for different time delays after near-infrared excitation. (a) The phase profiles from Figure 3b, and (b) Figure S3 are during the early and later times of the magnetization recovery process are shown.

References

1. Hill JP, McMorrow DF (1996) X-ray Resonant Exchange Scattering: Polariztaion Dependence and Correlation Function. *Acta Crystallogr Sect A Found Crystallogr* 52(2):236–244.

2. Millane RP, Arnal R, Chen J (2015) Phase retrieval for multiple objects. *SPIE Proceedings Volume 9600: Image Reconstruction from Incomplete Data VIII*, eds Bones PJ, Fiddy MA, Millane RP (San Diego, California, United States), p 960008.